

**Highly sensitive amperometric sensing of nitrite utilizing bulk-modified MnO₂ decorated
Graphene oxide nanocomposite screen-printed electrodes**

Nandita Jaiswal ^a, Ida Tiwari ^{a*}, Christopher W. Foster ^b, Craig E. Banks^b

*^aDepartment of Chemistry(Centre of Advanced Study), Institute of Science,
Banaras Hindu University, Varanasi, INDIA.*

*^bFaculty of Science and Engineering, Manchester Metropolitan University, Chester
Street, Manchester, M1 5GD, UK*

* Corresponding author:

Ida Tiwari: Tel: +91-9415813020; Fax: +91-542-2368174;

E-mail address: idatiwari@bhu.ac.in

Abstract

A screen-printed amperometric sensor based on carbon ink bulk-modified with MnO₂ decorated graphene oxide (MnO₂/GO-SPE) nanocomposite was investigated for its ability to serve as a sensor towards nitrite. The composite was prepared by simple ultrasonication and reflux methodology and was characterized by FT-IR spectroscopy, transmission electron microscopy, scanning electron microscopy, Raman spectroscopy, Atomic force microscopy and electrochemically using cyclic voltammetry, chronoamperometry and differential pulse voltammetry techniques. The MnO₂/GO-SPE was found to exhibit an electro-catalytic activity for the electrochemical oxidation of nitrite in 0.1 M phosphate buffer solution (pH 7.4). The electrochemical oxidation of nitrite occurs at +0.55 V (Vs. Ag/AgCl) with a limit of detection (3σ) found to be 0.09 μM and with two linear ranges of 0.1 μM to 1 μM and 1 μM to 1000 μM with sensitivities of 1.25 $\mu\text{A}\mu\text{M}^{-1}\text{cm}^{-2}$ and 0.005 $\mu\text{A}\mu\text{M}^{-1}\text{cm}^{-2}$ respectively. Furthermore, the MnO₂/GO-SPE showed an excellent anti-interference ability against a range of commonly encountered electroactive species and metal ions. Additionally, the fabricated MnO₂/GO-SPE nitrite sensor presented excellent selectivity, reproducibility and stability. The present study widens the scope of applications of graphene-based nanocomposite materials for on-site monitoring of nitrite.

Keywords: Nitrite, electroanalytical sensing, nanocomposite, screen-printed electrodes

1. Introduction

The last decades have witnessed an expansive interest in the detection and quantification of nitrite (NO_2^-) owing to the actuality of formation of carcinogenic nitrosamines by the interaction of nitrites with amines and also the oxidation of hemoglobin to methemoglobin, causing health issues such as methemoglobinemia [1,2]. Additionally, nitrite is customarily used as a preservative, dyeing agent, fertilizer and food additive. Thus, there is an imminent need for sensitive and rapid determination of NO_2^- for public health and environmental safety. Several approaches have been made for NO_2^- determination, such as spectrophotometry [3], chemiluminescence [4], ionic chromatography [5], high performance liquid chromatography [6,7], gas chromatography-mass spectrometry [8], capillary electrophoresis [9], spectrofluorimetry and electrochemical methods [10-12]. However, most of the predominantly reported techniques suffer from flaws such as use of toxic reagents, time consuming sample preparations, and susceptibility to potential interferences. Amongst all, the electrochemical mode has grabbed significant attention due to its high sensitivity, reliability, ease of operation, low cost, good selectivity, fast procedure, low detection limits and high accuracy [13, 14]. However, the electrochemical oxidation of nitrite at most common electrodes suffers from large overpotentials decreasing the sensitivity and accuracy of the electrodes which are easily affected by electroactive interferences. The surface modification of electrode has been adopted popularly to obtain a higher current response and to lower overpotential. In this context, the composites based on engineered carbon nano-materials are now days being principally used for designing electrochemical sensors/biosensors due to excellent electrochemical properties [15-19].

Graphene, a planar sheet of one-atom thickness sp^2 bonded carbon structure, due to its remarkable properties such as high specific surface area ($2630 \text{ m}^2 \text{ g}^{-1}$), high electronic conductivity (106 Scm^{-1}

¹), extraordinary electronic properties and a wide electrochemical window is foremost choice for electrochemical applications compared with those of other carbon based nano-materials, such as graphite and carbon nanotubes [20, 21]. Moreover, graphene oxide (GO), a decorated form of graphene with certain oxygen functionalities on the basal plane and edges provides strong hydrophilic properties and good dispersibility in water and other polar solvents. The main hindrance in the use of GO is due to the oxygen containing functional groups which result in loss in electrical conductivity as compared to graphene. This can be overcome by coupling GO with metal [22, 23], metal oxide [24, 25], metal hydroxide [26], metal sulfide [27] and noble metal nanoparticles [28–30] where GO provides large surface area for the immobilization of inorganic nano-particles to form composites with enhanced electrocatalytic performance. Amongst the library of many metal oxides, manganese dioxide (MnO_2) has gained much attention from researchers due to its low-cost, abundance and non-toxicity compared to other inorganic oxides such as cobalt, nickel and vanadium etc. [31, 32]. Moreover MnO_2 has superb electrocatalytic properties and fast response times and these properties have been utilized in supercapacitors but much less reports available in the field of electrochemical sensors and biosensors [33, 34]. The properties of MnO_2 depend on the manganese oxidation state and on the structural type of MnO_2 crystal; so great efforts have been made to prepare nano-crystalline MnO_2 with different structures.

In the present work, we have successfully exploited the unique features of GO and MnO_2 nano-particles to design a nanocomposite by simply decorating MnO_2 nanoparticles over GO sheet. The GO-wrapped MnO_2 nanocomposites were synthesized by co-assembly between MnO_2 nano-particles and negatively charged GO sheets. The process is thought to be driven by Van der Waals interactions [35]. More importantly, the presence of nano-structured MnO_2 is able to

efficiently prevent the aggregation of GO sheets caused due to the Van der Waals interactions, consequently leading to an increase in the available electrochemical active surface area and a suitable porous structure of MnO₂ nano-particles[36] facilitating easy approach of analyte. The electrochemical properties of the MnO₂ decorated graphene oxide nanocomposite (hereafter referred to as MnO₂/GO) were investigated in detail, and obtained results revealed that the composite material has a good electrochemical performance as electrode material. The as-fabricated MnO₂/GO nanocomposite was further incorporated in graphite ink and used for bulk production of screen-printed electrodes which are simple and disposable; yet sensitive, selective, and have lower overpotential for detection of nitrite in sub-millimolar levels as compared to prior reported works which suffer from low sensitivity, selectivity and lack of on-site applications [37-49]. The selectivity, operational stability and practicality of the developed nitrite sensor has also been critically assessed and demonstrated.

2. Experimental Section

2.1 Chemicals and reagents

Graphene oxide flakes, Chitosan (MW: 15000-20000), KMnO₄, oleic acid (C₁₈H₃₄O₂), sodium nitrite (NaNO₂), acetic acid (AcOH) were used and these chemicals were of analytical grade and purchased from Alfa-Aesar. All experiments were carried out in triple distilled water (tdw).

2.2 Methods

Preparation of dendrite shaped MnO₂

Dendrite shaped MnO₂ was prepared as reported in literature [36] with slight modifications. In a typical synthesis, 6.3 mmol of KMnO₄ was dissolved in 500 mL of triple distilled water and stirred

for 30 mins. Then, 10.0 mL of oleic acid (a capping agent) was added in the molar solution of KMnO_4 , and a steady emulsion was formed by vigorous stirring. The emulsion was transferred to a 1 L separating funnel and allowed to stand at room temperature for 24 hrs. A brown-black precipitate were collected on the organic layer which was separated from the aqueous layer and washed several times with ethanol to remove excess of oleic acid and then washed several times with distilled water. Finally, the precipitate was dried under a vacuum at $60\text{ }^\circ\text{C}$ for 10 hrs.

Synthesis of the MnO_2/GO nanocomposite

For the preparation of nanocomposite, GO was prepared by chemical oxidation and exfoliation of natural graphite performed according to modified Hummers method [50]. To an aqueous GO solution (1 mg/mL) prepared by ultrasonication, an equivalent amount of MnO_2 was added (for optimization data *cf.* table 1) and ultrasonicated for 2-3 hrs and then refluxed at high temperature for 10-12 h and the solid product was collected by centrifugation at 13,000 rpm and was dried under vacuum at $70\text{ }^\circ\text{C}$ for 12 hrs.

Fabrication of modified GC electrodes

The casting of MnO_2/GO nanocomposite on glassy carbon electrodes (GCE) was performed in a chitosan matrix (Chit) for which 0.1 g chitosan powder was mixed in 20 mL (0.2 M) AcOH solution and ultrasonicated for 30 mins. Then, 1 mg of MnO_2/GO nanocomposite was added to the Chit solution. The GCE was polished upto mirror finish using $0.05\text{ }\mu\text{m}$ alumina powder and was ultrasonicated in tdw and ethanol for 5 mins. $10\text{ }\mu\text{L}$ of the prepared $\text{MnO}_2/\text{GO}/\text{Chit}$ nanocomposite was drop-casted on the GCE and dried for 4-5 hrs and used further for electrochemical studies.

Preparation of Screen Printed Electrodes (SPE)

The in-house fabrication of screen-printed carbon electrodes were performed using suitable stencil designs using a microDEK1760RS screen-printing machine (DEK, Weymouth, UK). Firstly a

carbon–graphite ink formulation was screen-printed onto a flexible polyester film (Autostat, 250 micron thickness), then the layer was stored in a fan oven at 60 °C for 30 min. Ag/AgCl paste was screen printed for fabricating Ag/AgCl reference electrode (Gwent Electronic Materials Ltd, UK) onto the plastic substrate and the SPE was ready to use after a final coating of dielectric paste ink layer (Gwent Electronic Materials) to cover the connections and to define the graphite working electrode diameter to be 3 mm and cured for 30 min at 60 °C. The MnO₂/GO were incorporated into the SPEs according to % weight of M_P and M_I, where M_P is the mass of particulate and M_I is the mass of the carbon ink formulation used in the printing process. The weight per cent of M_P and M_I typically varied in the range of 0–10%. For the fabrication of the SPE, 0.75% (M_P/M_I) MnO₂/GO was used and screen-printed on top of the working electrode and cured as discussed above [51].

2.3 Instruments

The morphological investigations of MnO₂/GO have been carried out by the transmission electron microscope (TEM) using TECNAI 20G² FEI microscope (at 200 kV), SEM was performed with a Quanta200 FEI (13 kV), AFM images were obtained using Nova Px 3.1.0 Rev 3880, Raman spectra were recorded on a micro-Raman setup (Renishaw, UK) equipped with a grating of 2400 lines per mm and a Peltier cooled CCD, Thermogravimetric analysis (TGA) were performed using a Perkin Elmer (STA 6000) in the temperature range of 30 °C–900 °C and Fourier transform infrared (FT-IR) spectra were recorded on a Perkin Elmer (Spectrum Two) Fourier transform infrared spectrophotometer. Electrochemical analysis was conducted on a CHI 630C series (USA) electrochemical system with three-electrode cell using GCE as working electrode, platinum as auxiliary electrode and Ag/AgCl as reference electrode and SPE (screen printed electrodes) using onboard counter and reference electrodes (see earlier).

3. Result and Discussions

3.1 Physical Characterization

Transmission electron microscopy (TEM) studies

Fig.1 (A) depicts TEM images of MnO₂ nanoparticles where a polygonal structure with a size of 100nm is observed where MnO₂ nano-platelets are attached to each other to form nano-dendrites [36]. Fig. 1 (B) shows TEM image of GO which is as expected. Fig. 1(C) reveals the microstructural pattern of MnO₂/GO nanocomposite where it can be clearly seen that the MnO₂ nanoparticles are immobilized on the GO sheets. Furthermore, it can be inferred that the GO sheets [Fig. 1(B)] provide a surface for MnO₂ nanoparticles to be decorated upon. The selected area electron diffraction (SAED) pattern of MnO₂/GO [inset to Fig. 1(C)] exhibits a polycrystalline structure which corresponds to (002), (100), (110) plane of birnessite-type MnO₂ nanoparticles[36].

Scanning electron microscopy (SEM) studies

The surface morphology of MnO₂ nano-particles, GO, MnO₂/GO coated silver paste, were studied by SEM. Fig. 2(A) shows the flakes of GO, Fig. 2(B) shows the nearly spherical honeycomb structure of MnO₂ nano-particles [36] and Fig. 2(C) depicts the sheet of GO decorated with MnO₂ nano-particles. From the images it appears GO provides a suitable platform for the MnO₂ nano-particles to spread around. The presence of elements such as C, O, Mn in the composite has been confirmed using EDAX analysis [*cf.* Fig. 2(D)].

AFM studies

GO and MnO₂/GO coated glass was employed for the AFM analysis. Fig. 3(A) and (B) shows two and three dimensional view of GO and Fig. 3 (C) and (D) two and three dimensional view of MnO₂/GO nanocomposite respectively. Here the scan area was 1020 × 1020 nm and 1020 × 1020 nm. AFM tapping mode was applied for the surface morphological study. On comparing the Figs.3 (B) and (D), the decoration of MnO₂ nano-particles on the surface of GO sheet can be clearly

ascertained. Moreover, the average roughness for GO surface was found to be 0.306 nm and for MnO₂/GO to be 1.238 nm which further corroborates the findings that the nanocomposite material provides an increased surface area.

Raman Analysis

Raman spectroscopy is performed to identify the disorderness in the sp² carbon materials. The Fig. 4 (curve A) shows Raman spectra of GO where two distinct peaks at 1354 cm⁻¹ and 1596 cm⁻¹ are observed due to D-band caused by scattering of k-phonons of A_{1g} symmetry of the sp³ carbon structure and G-band due to first order scattering of E_{2g} phonons of sp² carbon structure respectively [52]. The Fig. 4 (curve B) shows a spectrum of the MnO₂/GO where shift in both D and G bands is apparent. The ratio of intensities of the D and G bands in the MnO₂/GO is found to be greater than that of GO, supporting the reduction of GO and its interaction with MnO₂ nanoparticles in the GO/MnO₂ nanocomposite [53].

FT-IR studies

The IR band of GO [Fig. 5, curve a] shows strong peak at 3400 cm⁻¹ corresponding to O-H vibration, at 1730 cm⁻¹ due to C=O stretching in COOH, at ~1300 and ~1060 cm⁻¹ due to C-O-C stretching vibrations and an additional peak at 1600 cm⁻¹ due to the unoxidised sp² domain of graphite.

The absorption bands due to interatomic vibration in metal oxides are generally observed below 1000 cm⁻¹[54]. In the Fig. 5, (curve b), vibrational peak for O-Mn is observed between 500-900 cm⁻¹[55]. The frequency of Mn-O symmetric stretch vibration was observed at 507 cm⁻¹, C-H vibration at 1421 cm⁻¹ and due to O-H stretching at 3400 cm⁻¹ in MnO₂ nanoparticles [36]. The bands of MnO₂/GO [Fig. 5, curve c] confirm an ample number of oxygen and carbon

functionalities of GO. Additionally the presence of vibration bands of MnO₂ nano-particles demonstrates the successful modification of the GO sheet by the nano-particles.

TGA analysis

To investigate the thermal properties of the MnO₂/GO nanocomposite and to study the influence of MnO₂ nano-particles on the thermal degradation behavior of GO, TGA was performed. Suppl. material Fig. 1 shows the weight loss curves for GO (curve a) and MnO₂/GO nanocomposite (curve b). Both the curves exhibit three-stage degradation behavior. From the curve (a) it can be seen that in GO in the first step, weight loss (~15%) is in the temperature range 30⁰C to 200⁰C, which might be due to a loss of moisture present within the sample. The second step shows a major weight loss (~21%) in the temperature range of 200⁰C to 300⁰C revealing the decomposition of labile oxygen functionalities such as carboxylic, anhydride, or lactones groups, from the surface of the GO sheets. The third step shows decomposition above 320⁰C which can be ascribed to the removal of more stable oxygen functionalities such as phenol, carbonyl and quinone. The thermal stability of the MnO₂/GO nanocomposite is better than that of GO (*c.f* Fig. 1 curve b). The results obtained show % weight loss for MnO₂/GO nanocomposite is less than that of GO proving that the thermal stability of GO is enhanced in presence of MnO₂ nano-particles.

3.2 Electrochemical characterization

Cyclic voltammetry (CV) is used to study the electrochemical behavior of GO, MnO₂, MnO₂/GO modified glassy carbon electrodes (GCE) in 0.1M, 7.4 PBS at 20 mVs⁻¹ using chitosan (chit) as a deposition matrix. The MnO₂/Chit (result not shown) and MnO₂/GO/Chit modified GCE exhibit redox peaks in the region +0.76 V and +0.40 V, which might be attributed to the redox nature of MnO₂. The suppl. material Fig. 2(A) shows CVs for MnO₂/GO/Chit modified GCE as a function

of scan rate for investigation of various kinetic parameters. The cathodic to anodic current (I_{pa}/I_{pc}) ratio was found to be greater than 1.0 implying that the process is not reversible further supported by the fact that the difference in peak potential (ΔE_p) is higher than 59mV (at 298K). The shift in the magnitude of I_{pa} and I_{pc} were observed to vary linearly with scan rate (v) (*cf.* inset I, suppl. Fig. 2 (A)) and follow the eqs. (1) and (2) confirming this to be a surface confined electrochemical phenomenon.

$$I_{pa}/A = 0.0134 v/mVs^{-1} + 1.0392 \quad [1] \quad R^2 = 0.996$$

$$I_{pc}/A = -0.0199 v/mVs^{-1} - 0.4887 \quad [2] \quad R^2 = 0.997$$

The redox potential were also found to increase linearly with $\log v$ following the equations (3) and (4) (*cf.* inset II, suppl. Fig. 2(A)) on GCE and the α value was calculated to be 0.67 and k_s value was found to be $2.08 s^{-1}$.

$$E_{pa}/V = 0.5040/V + 0.0434 \log v \quad [3] \quad R^2 = 0.995$$

$$E_{pc}/V = 0.4309/V - 0.0221 \log v \quad [4] \quad R^2 = 0.996$$

The electrochemical kinetic parameters were calculated using Laviron's eqns [56] (5) – (7):

$$E_{pa} = E^0 + \frac{2.303RT}{1-\alpha} nF \log v \quad [5]$$

$$E_{pc} = E^0 - \frac{2.303RT}{\alpha} nF \log v \quad [6]$$

$$\log k_s = \alpha \log(1 - \alpha) + (1 - \alpha) \log \alpha - \frac{\log RT}{nFv} - \frac{\alpha(1-\alpha)nF\Delta E_p}{2.303Rt} \quad [7]$$

The surface coverage of the electroactive nanocomposite on GCE was calculated using Laviron eqn.(8)

$$I_p = \frac{n^2 F^2 A \Gamma v}{4RT} \quad [8]$$

From the average value of cathodic and anodic results, the Γ value was found to be $8.8 \times 10^{-9} \text{ molcm}^{-2}$.

The suppl. material, Fig. 2(B) depicts CV of the MnO₂/GO-SPE in 0.1 M PBS (pH 7.4) over a range of scan rates. The redox peaks could not be observed clearly probably due to restricted movement of composite in graphite ink.

3.3 Electrocatalytic response of different modified GC electrodes towards NO₂⁻ oxidation

A comparative CV of GCE (inset), Chit/GCE, MnO₂ nano-particles/Chit-GCE, and MnO₂/GO/Chit-GCE in 0.1 M PBS (pH 7.4) [*cf.* Fig. 6] was performed to further confirm the electrocatalysis of NO₂⁻. A decrease in overpotential to +0.80V and an increase in the current is observed when the oxidation of NO₂⁻ is studied on MnO₂/GO/Chit-GCE (curve a). The GO/Chit-GCE (curve b) shows a broad irreversible peak for oxidation of NO₂⁻ at +0.96 V due to slow electron transfer kinetics whereas no such peaks were observed on MnO₂ nanoparticles/Chit-GCE (curve c) and Chit-GCE (curve d). Further, the electrocatalytic behaviour of the MnO₂/GO/Chit-GCE towards NO₂⁻ oxidation was studied at different scan rates 0.01 to 0.40 mVs⁻¹ in 0.1 PBS (pH 7.4) containing 0.5 mM of NO₂⁻ [*cf.* suppl. material; Fig. 3(A)]. The electrocatalytic oxidation process was found to be diffusion controlled with plots of I_p vs v^{1/2} and E_p vs log v linear in nature [*cf.* suppl. material; Fig. 3(B,C)]. The two Tafel slopes (b) and the transfer co-efficient (α) were found to be 96 mV, 160 mV and 0.53 respectively as reported in literature. To know the exact phenomenon occurring on MnO₂/GO/Chit-GCE, slope of the plot log I_p vs. log v was calculated which was found to be 0.38 further confirming the oxidation process to be diffusion controlled one [*cf.* suppl. material; Fig. 3(D)]. The electrochemical active surface area was calculated using eq. (9) [57] by comparing MnO₂ nano-particle/Chit-GCE, GO/Chit-GCE and MnO₂/GO/Chit-GCE in 0.1 M PBS (pH 7.4) towards 0.5mM NO₂⁻ oxidation:

$$I_p = 2.69 \times 10^5 n^{3/2} C_0 D^{1/2} A v^{1/2} \quad [9]$$

The electrochemical active surface area of MnO₂/GO/Chit-GCE was found to be approx 2.82 and 3.25 times than of MnO₂ nano-/Chit-GCE, and GO/Chit-GCE respectively.

3.4 Electrocatalytic response of the GO/MnO₂ modified SPE towards the sensing of NO₂⁻

For preparation and application of commercial electrodes for on-site monitoring of nitrite, the MnO₂/GO-SPEs were prepared and tested. Fig 7(A) shows the electrocatalytic response of 0.5 mM NO₂⁻ ion electrochemical oxidation on bare-SPE (curve a), MnO₂/GO-SPE (curve b), MnO₂/GO-GCE (curve c, inset) MnO₂/GO/Chit-GCE (curve d, inset), and MnO₂/GO/Chit-SPE (curve e, inset) in 0.1 M PBS (pH 7.4). No appreciable current was observed on bare-SPE (curve a) but maximum on MnO₂/GO-SPE (curve b). The response is minimum on MnO₂/GO-GCE (curve c, inset) due to continuous leaching of material. Hence, chitosan was used as a medium for dispersing and placing the prepared nanocomposite on GCE (curve d, inset).

On comparing the response on MnO₂/GO/chit-GCE (curve d, inset) and MnO₂/GO/chit-SPEs (curve e, inset) it was observed that the current was better and oxidation occurred at lower overpotential on MnO₂/GO/chit-SPEs but it shows broad oxidation peak which might be due to presence of two dispersants chitosan and carbon ink (required for bulk modification of SPE). To cut down this effect the chitosan was neglected in bulk modified MnO₂/GO-SPE. The results for NO₂⁻ oxidation showed a considerable decrease in overpotential to +0.55V towards NO₂⁻ oxidation at MnO₂/GO-SPEs and MnO₂/GO/Chit-SPEs. The best results were obtained on MnO₂/GO-SPE and MnO₂/GO/Chit-SPE with a decrease in oxidation potential of 200 mV with a 2 fold increase in the peak current for NO₂⁻ oxidation as compared to MnO₂/GO/Chit-GCE and MnO₂/GO-GCE, clearly indicating that the modified SPE facilitates electron transfer kinetics for faster NO₂⁻ oxidation. On comparing all the four electrodes prepared it can be concluded that MnO₂/GO/chit-

SPE showed oxidation at lowest overpotential with high sensitivity and reproducibility. Hence, it was used further for studies.

Fig. 7(B) shows differential pulse voltammetry response of NO_2^- oxidation on MnO_2/GO -SPE. Two linear calibration range is observed from 0.1 μM to 1 μM in lower range ($I_{\text{pa}}/\mu\text{A} = 4.5256C + 1.2591/\mu\text{M}$, $R^2 = 0.994$) (inset A) with and 1 μM to 1000 μM in higher range ($I_{\text{pa}}/\mu\text{A} = 6.1745C + 0.0054/\mu\text{M}$, $R^2 = 0.995$) (inset B) for NO_2^- oxidation in 0.1 M PBS (pH 7.4). Dual range in the determination of NO_2^- might be due to inevitable adsorption on of NO_2^- on MnO_2/GO -SPE surface as the concentration increases leading to hindered diffusion of analyte [58, 59]. The LOD is found to be 0.09 μM and the sensitivities to be 1.25 $\mu\text{A}\mu\text{M}^{-1}\text{cm}^{-2}$ and 0.005 $\mu\text{A}\mu\text{M}^{-1}\text{cm}^{-2}$ in ranges 0.1 μM to 1 μM and 1 μM to 1000 μM respectively [cf. Fig. 7(C)]. The results obtained are better/at par than most of the reported works as indicated in table 2, justifying the use of sensor for further technological applications.

3.5 Mechanism of electrocatalytic oxidation of NO_2^-

To gain acquaintance with the mechanism of the NO_2^- oxidation taking place at MnO_2/GO -SPE, CV at different scan rates in 0.1 M PBS, pH 7.4 containing 1 mM NO_2^- was recorded [cf. Fig. 8 (A)]. The NO_2^- oxidation current was found to be linear with respect to $v^{1/2}$ [cf. Fig. 8 A, inset] suggesting the process to be diffusion controlled. To ascertain the actual phenomenon occurring at MnO_2/GO -SPE surface the slope of the plot, $\log I_{\text{pa}}$ vs. $\log v$ was calculated [cf. Fig. 8 (B)]. Theoretically, for pure diffusional and adsorption process, the slopes of 0.5 and 1 respectively are observed [60, 61]. The process is said to be mixed adsorption-diffusion controlled if the value of the slope is in between 0.5-1, diffusion controlled if the slope value between 0.2-0.6, mixed diffusion-adsorption if between 0.6-0.75 and pure adsorption controlled when in between 0.75-1.0 [61]. Here the slope of the curve $\log I_{\text{pa}}$ vs. $\log v$ was found to be 0.48 which supports the fact

that the NO_2^- oxidation at $\text{MnO}_2/\text{GO-SPE}$ is diffusion controlled. Moreover, an increase in anodic peak potentials (E_{pa}) with increase in v is observed [*cf.* Fig. 8 (C)] which implies NO_2^- electrocatalytic oxidation is chemically irreversible process [62]. The value of Tafel slope (b) obtained from the plot of E_{pa} and $\log v$ were calculated to be 83 mV and 133mV from the slopes of eq. (10) and (11) confirming irreversible diffusive process as also previously reported [63]. The two linear plots obtained indicate a possibility of chemical reaction coupled with electrochemical reaction [62].

$$E_{pa}/V = 0.7227 + 0.0727 \log v \quad R^2 = 0.998 \quad [10]$$

$$E_{pa}/V = 0.7972 + 0.1421 \log v \quad R^2 = 0.996 \quad [11]$$

The number of electrons involved in the rate determining step can be obtained by using eq. (11),

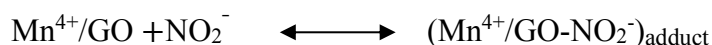
$$E_{pa} = \frac{b \log v}{2} + \text{constant} \quad [12]$$

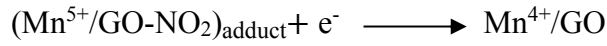
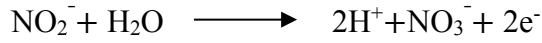
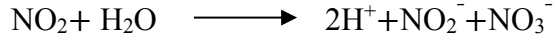
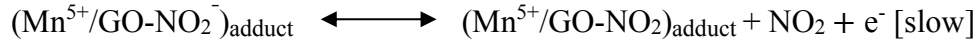
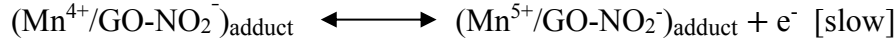
$$\text{Where } b = \frac{2.303RT}{(1-\alpha)n_{\alpha}F}$$

The terms E_{pa} , α , n_{α} , v stands for anodic peak potential, transfer coefficient, the number of electron involved in rate limiting step, scan rate respectively. On the basis of the b value and $n_{\alpha}= 1$, the value of α and $[(1-\alpha) n_{\alpha}]$ was calculated to be 0.62 and 0.38 respectively [63]. The number of overall electrons (n) involved in NO_2^- oxidation was calculated using slope of plot I_p vs. $v^{1/2}$ using eq. (12),

$$I_p = 2 \times 10^5 n [(1 - \alpha)n_{\alpha}]^{1/2} C_0 D^{1/2} A v^{1/2} \quad [13]$$

Where I_p , C_0 and D are anodic peak current, bulk concentration (molcm^{-3}) and diffusion coefficient respectively and other terms have their usual meaning. Using D value as $2.1 \times 10^{-5} \text{ cm}^2 \text{ s}^{-1}$ [64] the value of n was found to be 1.51 implying a two-electron transfer process. The proposed mechanism for NO_2^- oxidation might be the following reactions [63];





3.6 Kinetic studies by Chronoamperometry

To understand the kinetic process behind the electrocatalysis of NO_2^- , chronoamperometry was performed at +0.55 V, at which the analyte was best catalysed. The chronoamperograms for different aliquots of NO_2^- is shown in Fig. 9(A).

$$\frac{I_{\text{cat}}}{I_{\text{L}}} = (\pi t)^{1/2} (k_{\text{cat}} C_0)^{1/2} \quad [14]$$

The eq. (14) was used for calculating the catalytic rate constant, k_{cat} where I_{cat} and I_{L} are the current in presence and absence of NO_2^- and C_0 is bulk concentration. The value of k_{cat} was found to be $0.45 \times 10^5 \text{ mol}^{-1} \text{ cm}^3 \text{ s}^{-1}$ using the slopes of plot $I_{\text{cat}}/I_{\text{L}}$ vs. $t^{1/2}$ at 0.5mM of NO_2^- [cf. Fig. 9(B)] [65]. Moreover, the D value was calculated for NO_2^- oxidation using Cottrell equation;

$$I = nFD^{1/2}AC_0(\pi t)^{1/2} \quad [15]$$

The I vs. $t^{1/2}$ plot at different NO_2^- concentration exhibits a linear relationship [cf. Fig. 9(C)] and from the slope of the plot the average D value was calculated as $4.7 \times 10^{-5} \text{ cm}^2 \text{ s}^{-1}$ which is close to the reported value [66] and the slopes of each addition was in linear relation with the NO_2^- concentration [cf. Fig. 9(C), inset].

3.7 EIS study

The Fig. 10 represents the Nyquist diagrams of $\text{MnO}_2/\text{GO-SPE}$ both in the absence and presence of NO_2^- at 50, 100, 200, 300, 400 and 500 μM in 0.1 M PBS (pH 7.4). A semi-circle shaped curve is observed between the frequency range of 0.1 to 10^5 Hz in the absence of NO_2^- [cf. Fig. 10, curve

a] and with the increase of NO_2^- concentration a rational decrease in the diameter of the semi-circle is noticed [*cf.* Fig. 10 curve b-f]. This might be due to facilitated approach of NO_2^- at the active sites of the $\text{MnO}_2/\text{GO-SPE}$ which leads to the lowering of the charge transfer resistance (R_{ct}).

The equivalent electric circuits are usually applied to fit the experimental impedance spectra to interpret the electrochemical impedance results. The compatible equivalent circuit using Randles and Ershler model can be seen in Fig. 10 (inset), where R_{ct} , R_s and C represent charge transfer resistance, solution resistance and double layer capacitance (C_{dl}) respectively. The parallel combination (R_{ct} and C_{dl}) results in a depressed semi-circle in the Nyquist impedance plot with additions of NO_2^- .

$$R_{ct} = \frac{RT}{n^2 F^2 A k_{ct} [C_0]} \quad [16]$$

The relation between bulk concentration of NO_2^- and charge transfer resistance may be explained by equation (16), where R is the ideal gas constant, T is the absolute temperature, n is the number of transferred electrons per one molecule of the redox probe, F is faraday constant, A is geometric surface area of the electrode (cm^2), k_{ct} is potential dependent charge transfer rate constant and $[C_0]$ corresponds to the concentration of the redox probe (mol/cm^3) [67]. The R_{ct} for 0.1 M PBS solution $\{[\text{NO}_2^-] = 0\}$ is 483 $\text{K}\Omega$, which is much larger than that for 0.1 M PBS solution containing NO_2^- . Retrogression in the R_{ct} value is observed with the increase of NO_2^- concentration from 173 to 29.2 $\text{K}\Omega$. One may replace $[C_0] = k_1 [\text{NO}_2^-]$, where k_1 is a constant. If all other parameters are also constant, a linear relation [*cf.* Fig. 10 (B)] based on eq. (17), in which k_1 includes all constants is obtained.

$$\frac{1}{R_{ct}} = k_1 [\text{NO}_2^-] \quad [17]$$

The results obtained support the use of prepared nanocomposite for designing an impedimetric sensor in similar range as discussed above. After further addition of 500 μM there was no appreciable change in the resistance values possibly due to the saturation of active sites.

3.8 Optimization of various parameters

Variation of Composition

The effect of varying ratios of GO and MnO_2 nanoparticles in the MnO_2/GO nanocomposite can be observed from the Table 1 and their effect on the oxidation of 0.5 mM NO_2^- in suppl. material Fig. 4 bar graph I and II which proves 1 mg/mg MnO_2/GO is most suitable.

On the other hand, different amounts of MnO_2/GO nanocomposite dispersed in chit solution shows the maximum response for 0.5 mM NO_2^- oxidation at 1.0 mg of the nanocomposite [suppl. material Fig. 4 graph III] hence it was used in the experiments.

Variation of pH

The response for the anodic peak current for oxidation of NO_2^- was studied between the pH 4.0 to 9.0. (*cf.* suppl. material Fig. 5). MnO_2/GO -SPE showed maximum response in pH 7.4, 0.1 M PBS. At low pH the low anodic response for NO_2^- oxidation is observed due to conversion of NO_2^- ion into NO whereas at high pH the lack of proton leads to low anodic response because NO_2^- oxidation is based on proton availability [45]. So, pH 7.4 was chosen for the best sensor performance.

3.9 Selectivity and Stability of the Electrode

The selectivity of MnO_2/GO -SPE towards NO_2^- ions was examined by adding 100 folds of certain inorganic and organic compounds into the PBS (pH 7.4) containing 500 μM of NO_2^- . It was observed that change in the response caused by few species such as chloride ion (Cl^-), nitrate ion

(NO₃⁻), cysteine was more than 5% whereas less than 5% was observed in presence of other inferents such as sulphite (SO₃²⁻), sulphate (SO₄²⁻), tyrosine, dopamine, ascorbic acid, uric acid, and H₂O₂. The suppl. material Fig. 6 shows bar diagram for the modified SPE.

The stability of MnO₂/GO-SPE was obtained by studing the response for 0.5 mM NO₂⁻ in 0.1 M PBS (pH 7.4) at 20 mVs⁻¹ for 20 cycles and no appericiable decrease in the current was observed [suppl. material Fig. 7]. The MnO₂/GO-SPE were found to be stable even after 3-4 months of storage in air tight packings.

3.9. Real sample analysis

The practical applications of the sensor to detect NO₂⁻ in tap water and packaged water was assessed by standard addition method. Known amounts of NO₂⁻ were spiked in the tap water and packaged water. Excellent recovery was obtained by adding different concentration of NO₂⁻ in packaged water sample and tap water samples on MnO₂/GO-SPE can be seen from table 3.

4. Conclusion

A dendritic shaped MnO₂ nano-particles decorated GO nanocomposite was successfully synthesized using simple mechanical mixing and characterized using suitable analytical techniques. The MnO₂/GO-SPE was designed and fabricated for the electrochemical detection of nitrite. The MnO₂/GO-SPE exhibited an excellent electrocatalytic activity towards the oxidation of nitrite with a higher current and also significantly reduced overpotential as compared to the other electrodes due to synergistic effect between MnO₂ and GO. The sensor showed a linear oxidation current in the concentration range of 0.1 μM – 1 mM for nitrite, and the detection limit was found to be 0.09 μM. The excellent electrocatalytic activity, low detection limit, high sensitivity, rapid response time coupled with on-site monitoring feature makes it a potential candidate for commercialization.

Acknowledgments

N. J is thankful to UGC, New Delhi for awarding research fellowship. Authors are also thankful to Prof. O. N. Srivastava (Department of Physics, Institute of Science, B.H.U) for providing SEM and TEM facilities and Prof. Ranjan Singh (Department of Physics, Institute of Science, B.H.U) for Raman analysis.

References

- 1. Y. Li, H. Wang, X. Liu, L. Guo, X. Ji, L. Wang, D. Tian, X. Yang, Nonenzymatic nitrite sensor based on a titanium dioxide nanoparticles/ionic liquid composite electrode, J. Electroanal. Chem. 719 (2014) 35–40.**
- 2. K. Calfumána, M.J. Aguirreb, P.C. Rosales, S. Bolloc, R. Llusard, M. Isaacs, Electrocatalytic reduction of nitrite on tetraruthenatedmetalloporphyrins/Nafion glassy carbon modified electrode, Electrochim. Acta 56 (2011) 8484–8491.**
- 3. N. Pourreza, M.R. Fat'hi, A. Hatami, Indirect cloud point extraction and spectrophotometric determination of nitrite in water and meat products, Microchem. J. 104 (2012) 22–25.**
- 4. Z. Lin, W. Xue, H. Chen, J.M. Lin, Peroxynitrous-Acid-Induced Chemiluminescence of Fluorescent Carbon Dots for Nitrite Sensing, Anal. Chem. 83 (2011) 8245–8251.**
- 5. C. Abha, K.B. Anil, V.K. Gupta, Simultaneous determination of nitrite and nitrate by normal phase ion-pair liquid chromatography, Talanta 55 (2001) 789-797.**
- 6. H. Li , C.J. Meininger , G. Wu, Rapid determination of nitrite by reversed-phase high-performance liquid chromatography with fluorescence detection, J. Chromatogr B 746 (2000) 199–207.**

7. W.S. Jobgena, S.C. Jobgena, H. Li, C.J. Meiningerb, G. Wua, Analysis of nitrite and nitrate in biological samples using high-performance liquid chromatography, *J. Chromatogr. B* 851 (2007) 71–82.
8. M.S. Helmke, M.W. Duncan, Measurement of the NO metabolites, nitrite and nitrate, in human biological fluids by GC-MS, *J. Chromatogr. B* 851 (2007) 83-92.
9. T. Miyadoa, Y. Tanaka, H. Nagai, S. Takeda, K. Saitoc, K. Fukushi, Y. Yoshida, S. Wakida, E. Niki, Simultaneous determination of nitrate and nitrite in biological fluids by capillary electrophoresis and preliminary study on theirdetermination by microchip capillary electrophoresis *J. of Chromatogr. A* 1051 (2004) 185–191.
10. X. Ma, T. Miao, W. Zhu, X. Gao, C. Wang, C. Zhao, H. Ma, Electrochemical detection of nitrite based on glassy carbon electrode modified with gold–polyaniline–graphene nanocomposites, *RSC Adv.* 4 (2014) 57842–57849
11. B. Yuan, C. Xu, L. Liu, Y. Shi, S. Li, R. Zhang, D. Zhang, Polyethylenimine-bridged graphene oxide–gold film on glassy carbon electrode and its electrocatalytic activity toward nitrite and hydrogen peroxide, *Sens. Actuators B* 198 (2014) 55–61.
12. A. Ahami, F.S. Felehgari, T. Madrakian, H. Ghaedi, Surface decoration of multi-walled carbon nanotubes modified carbon paste electrode with gold nanoparticles for electro-oxidation and sensitive determination of nitrite, *Biosens. Bioelectron.* 51 (2014) 379–385.
13. J. R.C. da Rocha, L. Angnes, M. Bertotti, K. Araki, H. E. Toma, *Anal. Chim. Acta* 452 (2002) 23–28.
14. L. Fu, G. Lai, P. J. Mahon, J. Wang, D. Zhu, B. Jia, F. Malherbe, A. Yu, Carbon nanotube and graphene oxide directed electrochemical synthesis of silver dendrites, *RSC Adv.* 4 (2014) 39645–39650.

15. R.L. McCreery, **Advanced Carbon Electrode Materials for Molecular Electrochemistry**, *Chem. Rev.* **108** (2008) 2646–2687.
16. S.N. Kim, J.F. Rusling, F. Papadimitrakopoulos, **Carbon Nanotubes for Electronic and Electrochemical Detection of Biomolecules**, *Adv. Mater.* **19** (2007) 3214–3228.
17. L. Fu, J. Yong, G. Lai, T. Tamanna, S. Notley, A. Yu, **Nanocomposite Coating of Multilayered Carbon Nanotube–Titania**, *Mater. Manuf. Process* **29** (2014) 1030–1036.
18. L. Fu, G. Lai, H. Zhang, A. Yu, **One-Pot Synthesis of Multipod ZnO-Carbon Nanotube-Reduced Graphene Oxide Composites with High Performance in Photocatalysis**, *J. Nanosci. Nanotechnol.* **15** (2015) 4325–4331.
19. A. Yu, X. Zhang, H. Zhang, D. Han, A. R. Knight, **Preparation and electrochemical properties of gold nanoparticles containing carbon nanotubes-polyelectrolyte multilayer thin films**, *Electrochim. Acta* **56** (2011) 9015–9019.
20. Y. Wang, Y. Li, L. Tang, J. Lu, J. Li, **Application of graphene-modified electrode for selective detection of Dopamine**, *Electrochem. Commun.* **11** (2009) 889–892.
21. S. Alwarappan, A. Erdem, C. Liu, C.-Z. Li, **Probing the Electrochemical Properties of Graphene Nanosheets for Biosensing Applications**, *J. Phys. Chem. C* **113** (2009) 8853–8857.
22. X. Huang, S.Z. Li, S.X. Wu, Y.Z. Huang, F. Boey, C.L. Gan, H. Zhang, **Graphene oxide-templated synthesis of ultrathin or tadpole-shaped Au nanowires with alternating hcp and fcc domains**, *Adv. Mater.* **24** (2012) 979–983.
23. F.Y. Li, J.J. Zhao, Z.F. Chen, **Fe-anchored graphene oxide: a low-cost and easily accessible catalyst for low-temperature CO oxidation**, *J. Phys. Chem. C* **116** (2012) 2507–2514.
24. C.Z. Zhu, L. Han, P. Hu, S.J. Dong, **In situ loading of well-dispersed gold nanoparticles**

on two-dimensional graphene oxide/SiO₂ composite nanosheets and their catalytic properties, *Nanoscale* 4 (2012) 1641–1646.

25. B. Neppolian, A. Bruno, C.L. Bianchi, M. Ashokkumar, Graphene oxide based Pt–TiO₂ photocatalyst: ultrasound assisted synthesis, characterization and catalytic efficiency, *Ultrason. Sonochem.* 19 (2012) 9–15.

26. C. Nethravathi, M. Rajamathi, N. Ravishankar, L. Basit, C. Felser, Synthesis of graphene oxide-intercalated alpha-hydroxides by metathesis and their decomposition to graphene/metal oxide composites, *Carbon* 48 (2010) 4343–4350.

27. X.Q. Yin, T.S. Jiang, Q. Zhao, H.B. Yin, A facile synthesis of graphene-metal (Pb, Zn, Cd, Mn) sulfide composites, *J. Mater. Sci.* 47 (2012) 1026–1032.

28. S. Palanisamy, S. Ku, S.M. Chen, Dopamine sensor based on a glassy carbon electrode modified with a reduced graphene oxide and palladium nanoparticles composite, *Microchim. Acta* 180 (2013) 1037–1042.

29. H. Zhou, Y. Liu, W. Chi, C. Yu, Y. Yu, Preparation and antibacterial properties of Ag@polydopamine/graphene oxide sheet nanocomposite, *Appl. Surf. Sci.* 282 (2013) 181–185.

30. L. Fu, A. Yu, Electroanalysis of Dopamine Using Reduced Graphene Oxide Palladium Nanocomposites, *Nanosci. Nanotechnol. Lett.* 7 (2015) 147–151.

31. H. Prasad, R. Prasat, U. Hashim, A Review on the label free nanowire based biosensor, *J. Appl. Sci. Res.* 8 (2012) 4759–4769.

32. N.W. Beyene, P. Kotzian, K. Schachl, H. Alemu, E. Turkusic, A. Copra, H. Moderegger,

- I. Svancara, K. Vytras, K. Kalcher, (Bio)sensors based on manganese dioxide-modified carbon substrates: retrospections, further improvements and applications, *Talanta* 64 (2004) 1151–1159.
33. Y.H. Bai, J.J. Xu, H.Y. Chen, Selective sensing of cysteine on manganese dioxide nanowires and chitosan modified glassy carbon electrodes, *Biosens. Bioelectron.* 24 (2009), 2985-2990.
34. G. Yu, Q. Zhao, W. Wu, X. Wei, Q. Lu, A facile and practical biosensor for choline based on manganese dioxide nanoparticles synthesized in-situ at the surface of electrode by one-step electrodeposition, *Talanta* 146 (2016) 707–713.
35. Z. Wu, W. Ren, D. Wang, F. Li, B. Liu, H. Cheng, High-Energy MnO₂ Nanowire/Graphene and Graphene Asymmetric Electrochemical Capacitors *ACS Nano* 4 (2010) 5835-5842.
36. H. Chen, J. He, C. Zhang, Hong He, Self-Assembly of Novel Mesoporous Manganese Oxide Nanostructures and Their Application in Oxidative Decomposition of Formaldehyde, *J. Phys. Chem. C* 111 (2007) 18033-18038
37. M.A. Rahman, A. Pandikumar, N. Yusoff, N.M. Huang, H.N. Lim, Electrochemical sensing of nitrite using a glassy carbon electrode modified with reduced functionalized graphene oxide decorated with flower-like zinc oxide, *Microchim. Acta* 182 (2015) 1113–1122.
38. M.M. Shahid, P. Rameshkumar, A. Pandikumar, H.N. Lim, Y.H. Ng and N.M. Huang, An electrochemical sensing platform based on a reduced graphene oxide–cobalt oxide nanocube@platinum nanocomposite for nitric oxide detection, *J. Mater. Chem. A* 3 (2015) 14458–14468.

39. N. Yusoff, A. Pandikumar, A.R. Marlinda, N.M. Huang, H.N. Lim, Facile synthesis of nanosized graphene/Nafion hybrid materials and their application in electrochemical sensing of nitric oxide, *Anal. Methods* 7 (2015) 3537–3544.
40. V. Man, A.P. Periasamy, S.M. Chen, Highly selective amperometric nitrite sensor based on chemically reduced graphene oxide modified electrode. *Electrochem. Comm.* 17 (2012) 75-78.
41. R. Yue, Q. Lu, Y. Zhou, A novel nitrite biosensor based on single-layer grapheme nanoplatelet–protein composite film, *Biosens. And Bioelectron.* 26 (2011) 4436–4441.
42. S. Zhang, B.Q. Li and J.B. Zheng, An electrochemical sensor for the sensitive determination of nitrites based on Pt–PANI–graphene nanocomposites, *Anal. Methods* 7 (2015) 8366–8372.
43. X. Ma, T. Miao, W. Zhu, X. Gao, C. Wang, C. Zhaoa, H. Ma, Electrochemical detection of nitrite based on glassy carbon electrode modified with gold–polyaniline–graphene nanocomposites, *RSC Adv.* 4 (2014) 57842–57849
44. D. Ye, L. Luo, Y. Ding, Q. Chen, X. Liu, A novel nitrite sensor based on graphene/polypyrrole/chitosan nanocomposite modified glassy carbon electrode, *Analyst* 136 (2011) 4563–4569.
45. L. Fu, S. Yu, L. Thompsona, A. Yu, Development of a novel nitrite electrochemical sensor by stepwise in situ formation of palladium and reduced graphene oxide nanocomposites, *RSC Adv.* 5 (2015) 40111–40116.
46. S. Jiao, J. Jin, L. Wang, One-pot preparation of Au-RGO/PDDA nanocomposites and their application for nitrite sensing, *Sens. Actuators B* 208 (2015) 36–42.

47. C.E. Langley, B. Sljuki, C.E. Banks, R.G. Compton, Manganese Dioxide Graphite Composite Electrodes: Application to the Electroanalysis of Hydrogen Peroxide, Ascorbic Acid and Nitrite, *Anal. Sci.* 23 (2007) 165-170.
48. X. Huang, Y. Li, Y. Chen, L. Wang, Electrochemical determination of nitrite and iodate by use of gold nanoparticles/poly (3-methylthiophene) composites coated glassy carbon electrode, *Sens. Actuators, B* 134 (2008) 780-786.
49. C.Y. Lin, V.S. Vasantha, K.C. Ho, Detection of nitrite using poly(3,4-ethylenedioxythiophene) modified SPCEs, *Sens. Actuators B* 140 (2009) 51–57.
50. D.C. Marcano, D.V. Kosynkin, J.M. Berlin, A. Sinitskii, Z. Sun, A. Slesarev, L.B. Alemany, W. Lu, J.M. Tour, Improved synthesis of Graphene oxide, *ACS. Nano* 4 (2010) 4806-4814.
51. I. Tiwari, M. Singh, M. Gupta, J.P. Metters, C.E. Banks, Design of screen-printed bulk modified electrodes using anthraquinone–cysteamine functionalized gold nanoparticles and their application to the detection of dissolved oxygen, *Anal. Methods* 7 (2015) 2020–2027.
52. K.N. Kudin, B. Ozbas, H.C. Schniepp, R.K. Prud'homme, I.A. Aksay, R. Car, Raman Spectra of Graphite Oxide and Functionalized Graphene Sheets, *Nano Lett.* 8 (2007) 36–41.
53. T. Q. Xu, Q. L. Zhang, J. N. Zheng, Z.-Y. Lv, J. Wei, A. J. Wang, J. J. Feng, Simultaneous determination of dopamine and uric acid in the presence of ascorbic acid using Pt nanoparticles supported on reduced graphene oxide, *Electrochim. Acta* 115 (2014) 109-115.
54. C.N.R. Rao, Chemical applications of infrared spectroscopy, Academic Press, New York and London 1963.
55. H. Chen, J. He, Facile Synthesis of Monodisperse Manganese Oxide Nanostructures and Their Application in Water Treatment, *J. Phys. Chem. C* 112 (2008) 17540–17545.

56. E. Laviron, General expression of the linear potential sweep voltammogram in the case of diffusionless electrochemical systems, *J. Electroanal. Chem.* 101 (1979) 19–28.
57. Z. Miao, D. Zhang, Q. Chen, Non-enzymatic Hydrogen Peroxide Sensors Based on Multi-wall Carbon Nanotube/Pt Nanoparticle Nanohybrids, *Materials* 7 (2014) 2945-2955.
58. S. Zhang, B.Q. Li, J.B. Zheng, An electrochemical sensor for the sensitive determination of nitrites based on Pt–PANI–graphene nanocomposites, *Anal. Methods* 7 (2015) 8366–8372.
59. Y. Zhanga, Y. Zhaoa, S. Yuanb, H. Wanga, and C He, Electrocatalysis and detection of nitrite on a reduced graphene/Pd nanocomposite modified glassy carbon electrode, *Sens. Actuators B* 185 (2013) 602–607.
60. C. Batchelor-McAuley, L. M. Goncalves, L. Xiong, A. A. Barros , R. G. Compton, Controlling voltammetric responses by electrode modification; using adsorbed acetone to switch graphite surfaces between adsorptive and diffusive modes, *Chem. Commun.* 46 (2010) 9037–9039.
61. R. Gupta, S.K. Guin, S.K. Aggarwal, A mechanistic study on the electrocatalysis of the Pu(IV)/Pu(III) redox reaction at a platinum electrode modified with single-walled carbon nanotubes (SWCNTs) and polyaniline (PANI), *RSC Adv.* 2 (2012) 1810–1819.
62. C.A. Caro, F. Bedioui, J.H. Zagal, Electrocatalytic oxidation of nitrite on a vitreous carbon electrode modified with cobalt phthalocyanine, *Electrochim. Acta* 47 (2002) 1489–1494.
63. M.A. Kamyabi, F. Aghajanloo, Electrocatalytic oxidation and determination of nitrite on carbon paste electrode modified with oxovanadium (IV)-4-methyl salophen, *J. Electroanal. Chem.* 614 (2008) 157–165.
64. F. Matemadombo, T. Nyokong, Characterization of self-assembled monolayers of iron and cobalt octaalkylthiosubstituted phthalocyanines and their use in nitrite electrocatalytic oxidation, *Electrochim. Acta* 52 (2007) 6856–6864.

65. A.S. Adekunle, J. Pillay, K.I. Ozoemen, Probing the electrochemical behaviour of SWCNT–cobalt nanoparticles and their electrocatalytic activities towards the detection of nitrite at acidic and physiological pH conditions, *Electrochim. Acta* 55 (2010) 4319–4327.
66. M.H.P. Azar, H. Dastangoo, Electrocatalytic oxidation of nitrite at an aluminum electrode modified by a chemically deposited palladium pentacyanonitrosylferrate film, *J. Electroanal. Chem.* 567 (2004) 211–218.
67. H. Wang, H. Ohnuki, H. Endo, M. Izumi, Impedimetric and amperometric bifunctional glucose biosensor based on hybrid organic–inorganic thin films, *Bioelectrochem.* 101 (2015) 1–7.